The effect of stress on the magnetic properties of low bandwidth manganites

Guoqiang Song
East China Normal University
Yuanyuan Zhang (yyzhang@ee.ecnu.edu.cn)
East China Normal University https://orcid.org/0000-0002-3765-7298
Qingqing Liu
East China Normal University
Sheng Li
East China Normal University
Jing Yang
east china normal university
Wei Bai
East China Normal University
Xiaodong Tang
East China Normal University

Research Article

Keywords: manganese, stress, anisotropic, photoinduced magnetization.

Posted Date: March 18th, 2021

DOI: https://doi.org/10.21203/rs.3.rs-314141/v1

Version of Record: A version of this preprint was published at Journal of Materials Science: Materials in Electronics on August 14th, 2021. See the published version at https://doi.org/10.1007/s10854-021-06796-4.

Abstract

The low bandwidth $Pr_{0.9}Ca_{0.1}MnO_3$ (PCMO) thin films prepared by sol-gel method were suffered tensile and compressive stress grown on $SrTiO_3$ and $LaAlO_3$ substrates. The hysteresis loops at different temperatures show that the coercivity field with tensile stress is larger due to the much stronger pinning potential of ferromagnetism motion. The temperature dependence of the ZFC and FC magnetizations indicates that the stress significantly affects the ferromagnetic (FM) and antiferromagnetic (AFM) transition temperature of PCMO, and the Curie temperature (T_C) decreases with tensile stress. The films show strong anisotropy properties that the magnetization increases much faster with the magnetic field when $H \perp c$, but the coercive field and saturation magnetization do not change significantly. In addition, the persistent photoinduced magnetization is investigated, and significant improvement of the ferromagnetic ordering was observed in low temperature.

1. Introduction

The perovskite manganese oxide with the general formula $R_{1-x}A_xMnO_3$ (R = La, Pr, Nd, etc., A = Ca, Sr, Ba, etc.) has a high correlation between charge, spin, lattice, and orbital degrees of freedom, which leads to a variety of exotic behavior, such as colossal magnetoresistance (CMR), photoinduced change of magnetization and resistivity, etc [1–4]. It is not only interesting from the application point of view but also broadens the scientific understanding about the material properties. The low bandwidth $Pr_{1-x}Ca_xMnO_3$ (PCMO) is especially interesting due to the multiple magnetic phases and sensitive magnetic properties [5–8]. At the low-hole doping content $x = 0.1$, the valence states of Mn are mixed, and both the ferromagnetic (FM) and antiferromagnetic (AFM) phases coexist in the ground state [9]. The double exchange interaction between these Mn^{3+} and Mn^{4+} leads to FM, whereas the superexchange interaction between Mn^{3+}-Mn^{3+} and Mn^{4+}-Mn^{4+} leads to AFM ordering in manganites oxides [10]. The structure, both the Mn-O-Mn bond length and angle, will strongly affect the electronic transition between Mn^{3+} and Mn^{4+}, thereby changing its magnetic properties. Meanwhile, stress is an effective means to control the crystal structure of manganese oxide [11–13]. The epitaxial film on different substrates can control the transition from compressive stress to tensile stress, affect its Mn-O bond and regulate magnetic properties. The changes in magnetic properties caused by the structure will inevitably be reflected in the anisotropic physical properties [14–15]. The low doped PCMO films also have a great magnetization change under light [10, 16, 17]. Light can change the FM domain motion or volume fraction in AFM matrix, which leads to the change of magnetization signal. Although relevant researches have been done, there is few reports on the stress effect systemically on magnetic and magneto-optical properties.

In this paper, in order to attain a detailed understanding of the substrate-induced strain effects in *c*-axis-oriented $Pr_{1-x}Ca_xMnO_3$ (PCMO) films, we used $SrTiO_3$ (STO) and $LaAlO_3$ (LAO) single crystals as substrates and studied the effects of substrate-induced strain on the magnetic properties, anisotropic and photoinduced magnetization of PCMO films. The experimental results indicate that, the in-plane tensile strain was 0.60% for PCMO/STO films and the in-plane compressive strain in the film was 0.21% for

PCMO/LAO films respectively. It is giving rise to the distortion of MnO_6 octahedra and an increase of T_C by 3 K. At the same time, the magnetization of FM state is strengthened by the compressive strain while photoinduced magnetization in the AFM state is enhanced. The strain effects are found to be closely related to the Jahn-Teller electron-lattice coupling linked to magnetic properties.

2. Experimental Details

PCMO thin films were prepared on sol-gel method on $SrTiO_3$ (STO) (100) substrates and $LaAlO_3$ (LAO) (100) substrates. Praseodymium acetate [$Pr(CH_3COO)_3$], Calcium acetate [$Ca(CH_3COO)_2{\cdot}H_2O$] and Manganous acetate [$C_6H_9MnO_6{\cdot}2H_2O$] were dissolved into a solvent containing acetic acid (CH_3COOH), deionized water and acetylacetonate to prepare the precursor solution. The rotation speed and the spin time were at 5000 rpm and 30 s, respectively. After coating each layer, the film was fired at 200^{o}C for 180 s, then pyrolyzed at 400^{o}C for 180 s, and finally annealed at 850^{o}C for 600 s. The cycle was repeated several times in order to get films with a final thickness around 120 nm. Detailed information about material preparation and the structural properties of the film has been reported in our previous correspondence [18].The phase purity and structure of the films were measured q-2q and reciprocal space mapping by high-resolution X-ray diffraction (HRXRD, Bruker D8 Discover, Germany). Superconducting quantum interference device (SQUID, Quantum Design, USA) magnetometer was used for the magnetization characterization. The magnetic field is usually perpendicular to the out-of-plane of the thin film besides both perpendicular and parallel direction in magnetic anisotropy part. The magneto-optical magnetization was made for the sample in the dark and illumination with the magnetic field parallel to the out-of-plane of the thin film and laser working at l = 500 nm by the FOSH option of the SQUID.

3. Results And Discussion

Figure 1 (a) shows the q-2q patterns of PCMO films grown on both substrates. It is observed only the (00*l*) diffraction peaks of the PCMO films and the substrates, which means the phase purity and the epitaxial grown of the PCMO films on both STO and LAO substrates. Compared with the sample PCMO/LAO, the (002) diffraction peak of the PCMO/STO shifts to a higher angle, which indicates that the out-of-plane lattice parameters of PCMO/LAO is larger. The lattice parameter of PCMO ceramics (0.3854nm) is between the STO substrate (0.3905nm) and the LAO substrate (0.3792nm), which makes the PCMO subject to different stresses on these two substrates. The presence of stress will cause distortion of the lattice structure, affect the bond length and bond angle of Mn-O-Mn, and then change the magnetic properties of PCMO. The stress state of the film can also be seen through reciprocal space mapping in Fig. 1 (b) and (c). The abscissa of PCMO/STO film is almost consistent with that of substrate, indicating that the sample is in stress bound state, while that of PCMO/LAO has a certain deviation, which indicates that the structure relaxation of the film. The calculated values of the lattice parameters are the following, a = 0.3846nm, c = 0.3859nm (PCMO/LAO), and a = 0.3877nm, c = 0.3845nm (PCMO/STO) [19, 20]. This indicates that in the in-plane direction PCMO/LAO is under compression strain

while PCMO/STO is under tensile strain. The strain will result in the distortion of the lattice structure and change the lattice constant of the MnO_6 octahedra. Hence, the magnetic properties will be discussed in detail due to the different stress states of PCMO grown on LAO and STO substrates.

The *M-H* curves of both PCMO/LAO and PCMO/STO at different temperatures are shown in Fig. 2. The saturation magnetization is almost the same at different temperatures, while the coercive field and remanent magnetization decrease with the increase of temperature. The temperature dependence of coercive field (Fig. 2c) shows that the coercive field of PCMO/LAO is smaller than PCMO/STO, but the change trend is similar. At 5K, the coercive field is 760 Oe and 870 Oe for PCMO/LAO and PCMO/STO, respectively. However, the coercive field of the two substrates is similar at 50K, about 300Oe. The temperature dependence of the coercivity is related to the competition between AFM and FM in the spin-glass (SG) state [21]. In the ground state, the AFM and FM phases are coexisted in our low doped manganites. As PCMO/STO is subjected to tensile from the substrate, thereby static lattice stress increases the Mn–O bond length while decreasing the Mn-O-Mn bond angle [22, 23]. Tensile strain suppresses ferromagnetism by a strain induced distortion of MnO_6 octahedra. This leads to the enhancement of the pinning effect of the AFM phase fraction on the FM domain movement in the PCMO/STO film, thereby observing a higher coercive field at low temperatures [24, 25]. As the temperature gradually approaches the Neel temperature (T_N), the volume fraction of AFM begins to decrease, the pinning effect weakens, and the coil begins to become sharper. On the other hand, the coercive field of PCMO/LAO is smaller, which may be due to the weaker pinning effect caused by the in-plane compressive stress. When the temperature rises, the SG state gradually disappears, and the gap between the films on two kinds of substrate is no longer obvious.

To observe the relationship between stress and AFM-FM phase transition, we have measured the zero field cooling (ZFC) and field cooling (FC) magnetization of PCMO/STO and PCMO/LAO under series applied magnetic fields in Fig. 3(a) and Fig. 3(b). It can be observed that the magnetization increases rapidly with the decrease of temperature below 120K, which indicates that PCMO films begin to transform from paramagnetic state to FM state. As the temperature decreases more, the ZFC magnetization begins to decrease. The result shows that AFM phase and FM phase coexist in PCMO films at low temperature [21, 25]. Comparing the *M-T* curves of PCMO/STO and PCMO/LAO (Fig. 3(c)), the magnetization of PCMO/STO is much smaller than that of PCMO/LAO. The phenomenon may be due to tensile strain suppresses ferromagnetism in CMR thin films [23]. Figure 3(d) shows the dependence of T_C and T_N on magnetic field for the two samples. The tensile strain reduces the T_C of PCMO by 3K compared with the compressive strain. It is generally caused by the strain induced distortion of MnO_6 octahedra [26]. For PCMO thin films in both stress states, the T_N shifts towards lower temperature for higher applied magnetic field. As the magnetic field increases to 1000Oe, T_N of PCMO/LAO and PCMO/STO is close (about 45K), which is consistent with the phenomenon that the coercive field is equal at 50K observed in Fig. 2. When the magnetic field is lower than the coercive field, the T_N is affected by the stress as the same trend with T_C. However, when the magnetic field is higher than the coercive field, the T_N of PCMO with tensile stress is higher than that with compressive stress. Besides the phase transition temperature

both T_C and T_N, the magnetic moments below T_C of PCMO with tensile stress is smaller than that with compressive stress due to the distortion of MnO_6 octahedron.

In order to better understand the magnetic properties of PCMO, we studied the magnetic anisotropy of PCMO films. The hysteresis loops of PCMO/LAO at two directions are shown in Fig. 4(a). The magnetization curves show clear anisotropy behavior at lower fields and isotropic at higher fields. Along $H \perp c$ direction, the magnetization increases steeply at low fields (< 20 kOe), and gradually reaches saturation with the increase of magnetic field. It is clear that the in-plane magnetization ($H \perp c$) is now much easier to be saturated than the perpendicular magnetization [27]. For PCMO/LAO, the in-plane lattice is under compressive strain which will intensify the distortion of MnO_6 octahedra, and the [00*l*] lattice direction is the easy axis for the magnetocrystalline anisotropy of PCMO/LAO films [28, 29]. Although the magnetization of two directions changed obviously, we observed that the coercive field H_C was almost the same, indicating that magnetic anisotropy has a correspondingly negligible effect on pinning potential of FM domain. Figure 4(b) shows the temperature dependence of the magnetization under 500 Oe magnetic field. In addition, T_N of PCMO/LAO along easy axis is slight lower than that in hard axis.

Figure 5(a) shows the *M-H* curve under light and dark, which indicting that the curve became a little sharper with the application of light. The inset of Fig. 5(a) shows that the coercivity field decreases under illumination which was explained by the improvement of domain shift of FM clusters [25]. AFM and FM coexist in PCMO thin films at low temperatures, resulting in a SG state at low temperature [21]. The lattice parameters of these coexisting AFM and FM domains are slightly different which create a blocking strain. The blocking strain makes FM domain face a lot of pinning potential. When we add external light to the system, the light can provide energy to the system to overcome the pinning potential [21, 25]. To observe the photoinduced magnetization with temperature, the ZFC and FC curves were characterized in the dark and during illumination of PCMO/LAO under 1000 Oe and 1500 Oe magnetic field as shown in Fig. 5 (b) and (c), respectively. The magnetization of ZFC was lager under light at low temperature, but the magnetization of FC was inhibited under light. In order to better analyze this phenomenon, we compared the magnetization of ZFC and FC under light and dark conditions. Figure 5d shows plots of

$$\Delta M^{ZFC} = M_{\text{light}}^{ZFC} - M_{dark}^{ZFC} \text{ and } \Delta M^{FC} = M_{\text{light}}^{FC} - M_{\text{dark}}^{FC}$$

as functions of temperature. The magnetic moment during the ZFC process increases significantly under illumination, showing a good photoinduced magnetization effect. However, the magnetization of FC was inhibited under light. This clearly signifies that light can provide energy to overcome the blocking strain produced by AFM and FM domain and improve the FM interaction. However, due to the large JT distortion of PCMO, the 2p(O)→3d(Mn) charge transfer energy can be increased significantly, and the energy provided by light can not induce the charge transfer process. The content of Mn^{3+} in PCMO will increase slightly, and a small amount of electrons may be transferred to Mn^{4+} [30]. The increase of Mn^{3+} ions and

the decrease of hole concentration under illumination actually increases AFM Mn^{3+}-Mn^{3+} super-exchange interaction and weakens the FM-DE interaction which reduces the saturation moment of FC [25].

4. Conclusion

In conclusion, the low-bandwidth manganite $Pr_{1-x}Ca_xMnO_3$ ($x = 0.1$) thin films with both tensile and compressive stress were prepared by sol-gel method on STO and LAO single crystal substrates. Stress can affect the lattice structure of PCMO. Static lattice compression can reduce the Mn-O bond length and increase the Mn-O-Mn bond angle. It shows larger coercive field and smaller saturation magnetization for PCMO/STO with tensile stress. The T_C of the films is decreased by tensile strain. In addition, compared with compressive strain, tensile strain decreases T_N at low magnetic field, but increases at high magnetic field. It shows clearly magnetic anisotropy for the PCMO/LAO, and the [00*l*] lattice direction is the easy axis. Under light irradiation, the ZFC magnetization of PCMO overcomes the pinning potential of FM domain and improves the ordering of FM domain, which leads to the significant increase of ZFC magnetization. However, the decrease of FC magnetization under illumination indicates that the increase of Mn^{3+} ion concentration weakens the double-exchange interaction and suppresses the FM ordering. This research on the magnetization characteristics of PCMO films on different substrates provides useful information for device applications.

Declarations

Acknowledgements

This work is supported by the National Key Research and Development Program of China (2017YFA0303403), the National Natural Science Foundation of China (61674058, 61574058).

References

1. S. Rajpurohit, L.Z. Tan, C. Jooss and P.E. Blöchl, Phys. Rev. B **102**, 174430 (2020).
2. A. Swain, P.S. Anil Kumar and V. Gorige, J. Magn. Magn. Mater. **485**, 358-368 (2019).
3. M.J. Myron B. Salamon, Rev. Mod. Phys. **73**, 583 (2001).
4. T.H. Elbio Dagotto, Adriana Moreo, Physics Reports **344**, 153 (2001).
5. T. Elovaara, J. Tikkanen, S. Granroth, S. Majumdar, R. Felix, H. Huhtinen and P. Paturi, J. Phys.-Condes. Matter **29**, 425802 (2017).
6. Y.L. Wang, M.F. Liu, Y.L. Xie, Z.B. Yan, S. Dong and J.M. Liu, J. Appl. Phys. **118**, 123901 (2015).
7. T. Li, A. Patz, L. Mouchliadis, J. Yan, T.A. Lograsso, I.E. Perakis and J. Wang, Nature **496**, 69-73 (2013).
8. P. Beaud, A. Caviezel, S.O. Mariager, L. Rettig, G. Ingold, C. Dornes, S.W. Huang, J.A. Johnson, M. Radovic, T. Huber, T. Kubacka, A. Ferrer, H.T. Lemke, M. Chollet, D. Zhu, J.M. Glownia, M. Sikorski, A.

Robert, H. Wadati, M. Nakamura, M. Kawasaki, Y. Tokura, S.L. Johnson and U. Staub, Nat. Mater. **13**, 923-927 (2014).

9. T. Elovaara, S. Majumdar, H. Huhtinen and P. Paturi, Adv. Funct. Mater. **25**, 5030-5037 (2015).
10. S. Majumdar, H. Huhtinen, M. Svedberg, P. Paturi, S. Granroth and K. Kooser, J. Phys.-Condes. Matter **23**, 466002 (2011).
11. A. Tebano, C. Aruta, S. Sanna, P.G. Medaglia, G. Balestrino, A.A. Sidorenko, R. De Renzi, G. Ghiringhelli, L. Braicovich, V. Bisogni and N.B. Brookes, Phys. Rev. Lett. **100**, 137401 (2008).
12. F. Yang, N. Kemik, M.D. Biegalski, H.M. Christen, E. Arenholz and Y. Takamura, Appl. Phys. Lett. **97**, 092503 (2010).
13. E.J. Moon, P.V. Balachandran, B.J. Kirby, D.J. Keavney, R.J. Sichel-Tissot, C.M. Schlepütz, E. Karapetrova, X.M. Cheng, J.M. Rondinelli and S.J. May, Nano Lett. **14**, 2509-2514 (2014).
14. Y. Okimoto, Y. Tomioka, Y. Onose, Y. Otsuka and Y. Tokura, Phys. Rev. B **59**, 7401-7408 (1999).
15. S. Yamada, T. Matsunaga, E. Sugano, H. Sagayama, S. Konno, S. Nishiyama, Y. Watanabe and T.-h. Arima, Phys. Rev. B **75**, 214431 (2007).
16. S. Majumdar, T. Elovaara, H. Huhtinen, S. Granroth and P. Paturi, Journal of Applied Physics **113**, 063906 (2013).
17. S. Majumdar, H. Huhtinen, T. Elovaara and P. Paturi, J. Supercond. Nov. Magn **28**, 197-201 (2015).
18. Q. Ren, Y. Zhang, Y. Chen, G. Wang, X. Dong and X. Tang, J. Sol-Gel Sci. Technol. **67**, 170-174 (2013).
19. J. Zhang, H. Tanaka, T. Kanki, J.-H. Choi and T. Kawai, Phys. Rev. B **64**, 184404 (2001).
20. M.B. Salamon and M. Jaime, Rev. Mod. Phys. **73**, 583-628 (2001).
21. M. Svedberg, S. Majumdar, H. Huhtinen, P. Paturi and S. Granroth, J. Phys.-Condes. Matter **23**, 386005 (2011).
22. J.M. De Teresa, M.R. Ibarra, J. Blasco, J. García, C. Marquina, P.A. Algarabel, Z. Arnold, K. Kamenev, C. Ritter and R. von Helmolt, Phys. Rev. B **54**, 1187-1193 (1996).
23. R.A. Rao, D. Lavric, T.K. Nath, C.B. Eom, L. Wu and F. Tsui, Appl. Phys. Lett. **73**, 3294-3296 (1998).
24. A.K. Nayak, C. Shekhar, J. Winterlik, A. Gupta and C. Felser, Appl. Phys. Lett. **100**, 152404 (2012).
25. S. Majumdar, H. Huhtinen, M. Svedberg, P. Paturi, S. Granroth and K. Kooser, J. Phys.-Condes. Matter **23**, 466002 (2011).
26. A.J. Millis, T. Darling and A. Migliori, J. Appl. Phys. **83**, 1588-1591 (1998).
27. Z.-H. Wang, G. Cristiani, H.U. Habermeier, Z.-R. Zhang and B.-S. Han, J. Appl. Phys. **94**, 5417 (2003).
28. L.M. Berndt, V. Balbarin and Y. Suzuki, Appl. Phys. Lett. **77**, 2903-2905 (2000).
29. K. Okada and S. Yamada, Phys. Rev. B **86**, 064430 (2012).
30. S. Majumdar, H. Huhtinen, T. Elovaara and P. Paturi, J. Supercond. Nov. Magn **28**, 197-201 (2015)

Figures

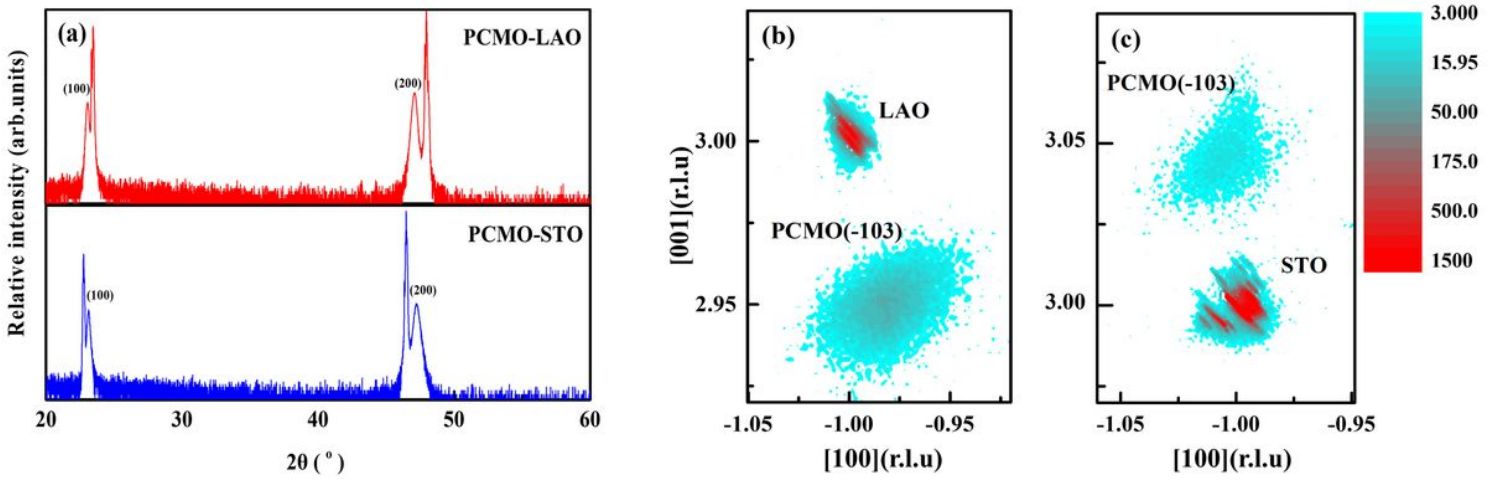

Figure 1

(a) XRD patterns of PCMO films grown on (001) LaAlO3 and (001) SrTiO3 substrates. Reciprocal space maps around the (-103) reflection of (b) PCMO/LAO and (c) PCMO/STO.

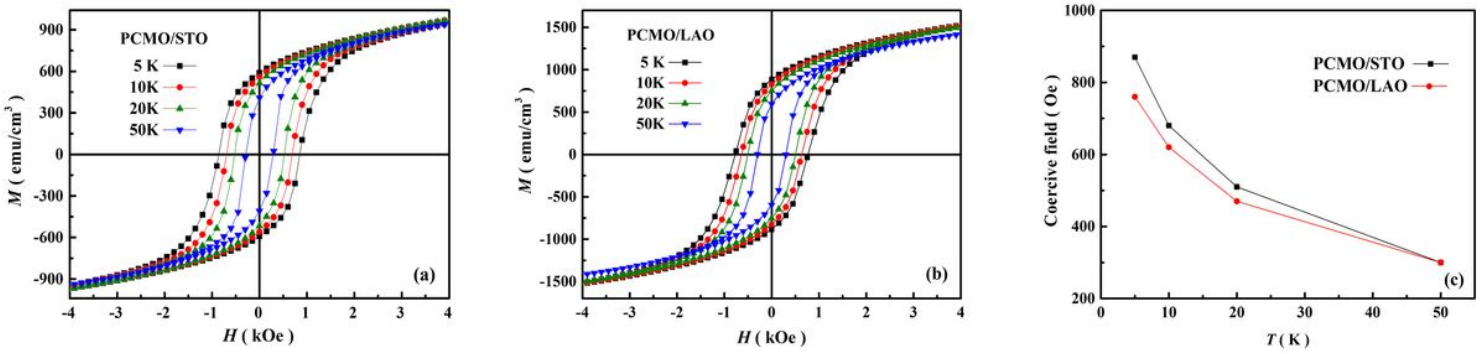

Figure 2

Magnetic hysteresis loops measured at temperatures of 5 K, 10 K, 20 K and 50 K of PCMO/STO (a) and PCMO/LAO (b). (c) The temperature dependence of the coercive field HC.

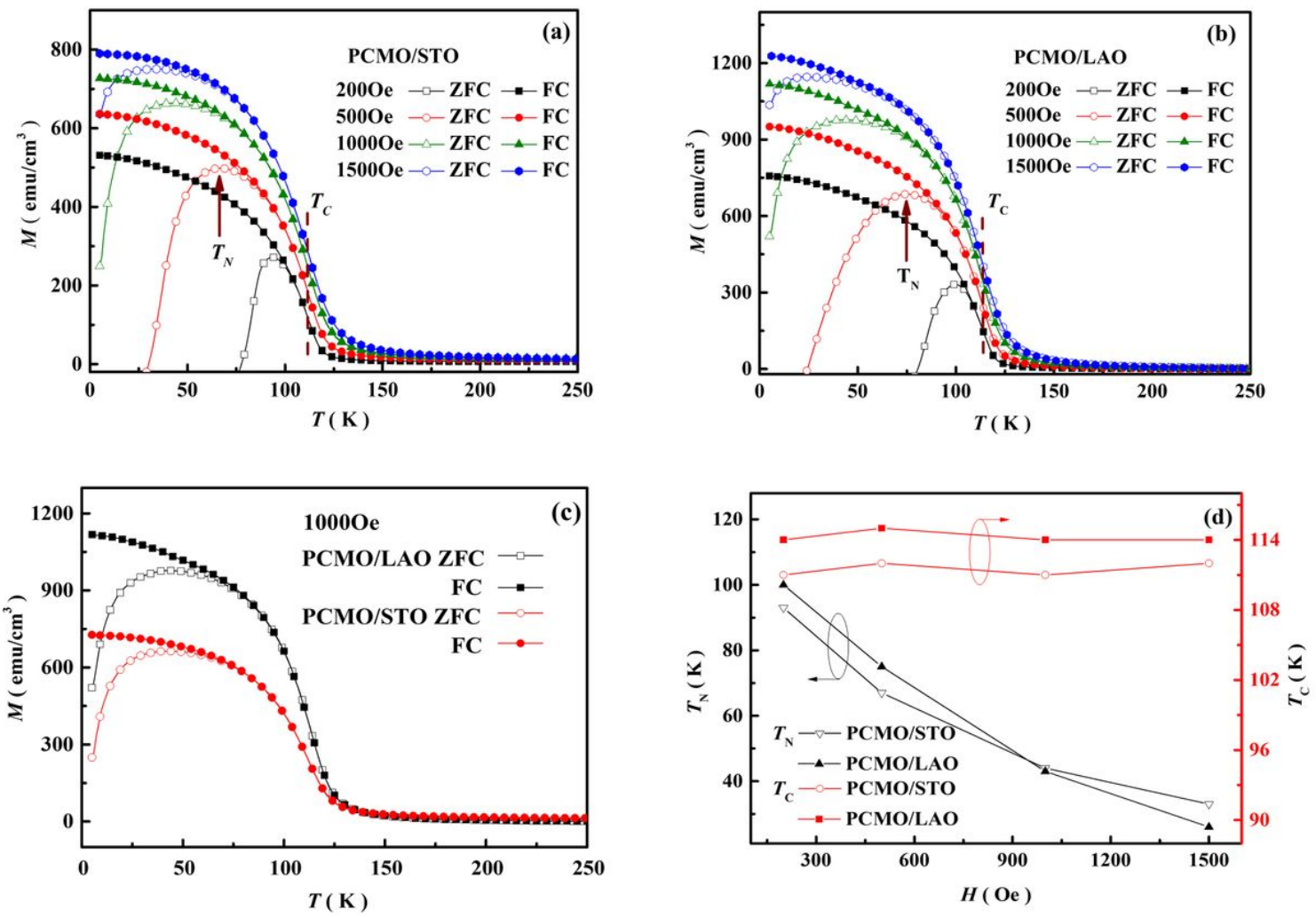

Figure 3

The temperature dependence of the ZFC and FC magnetizations measured in different magnetic fields of PCMO/STO (a) and PCMO/LAO (b). (c) The contrast of M-T curves of PCMO / LAO and PCMO/STO in the external magnetic field of 1000Oe. (d) The magnetic field dependence of TC and TN of PCMO.

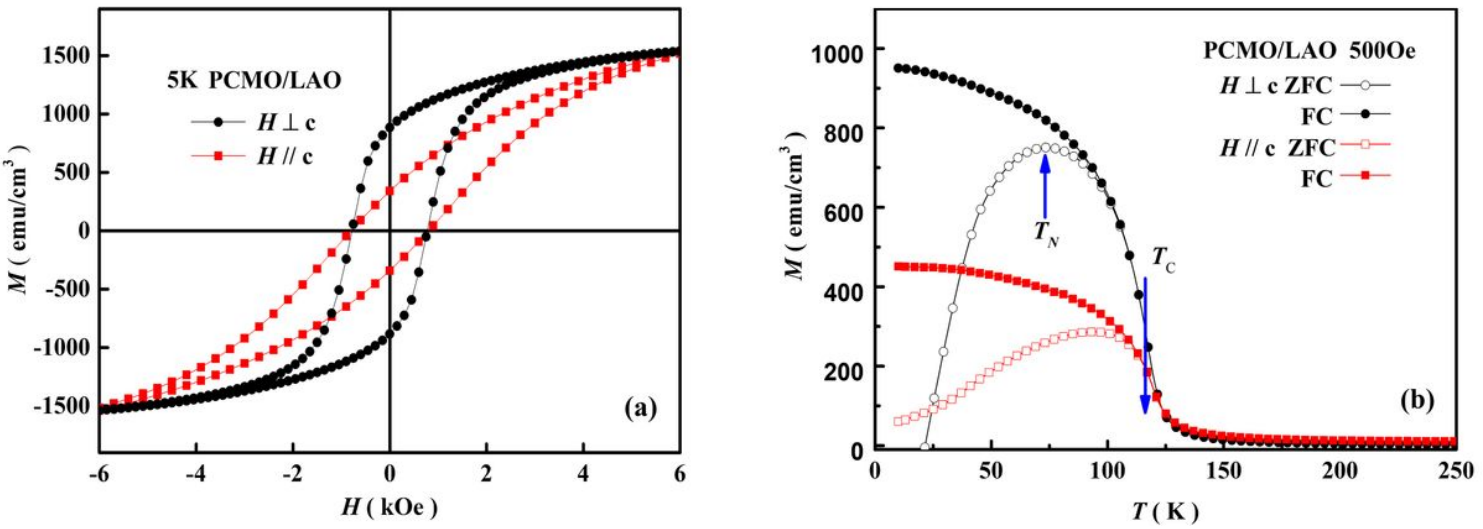

Figure 4

(a)The hysteresis loops of PCMO/LAO measured between -6 and 6 kOe magnetic fields in H⊥c and H//c.
(b)The temperature dependence of the ZFC and FC magnetizations measured in H⊥c and H//c.

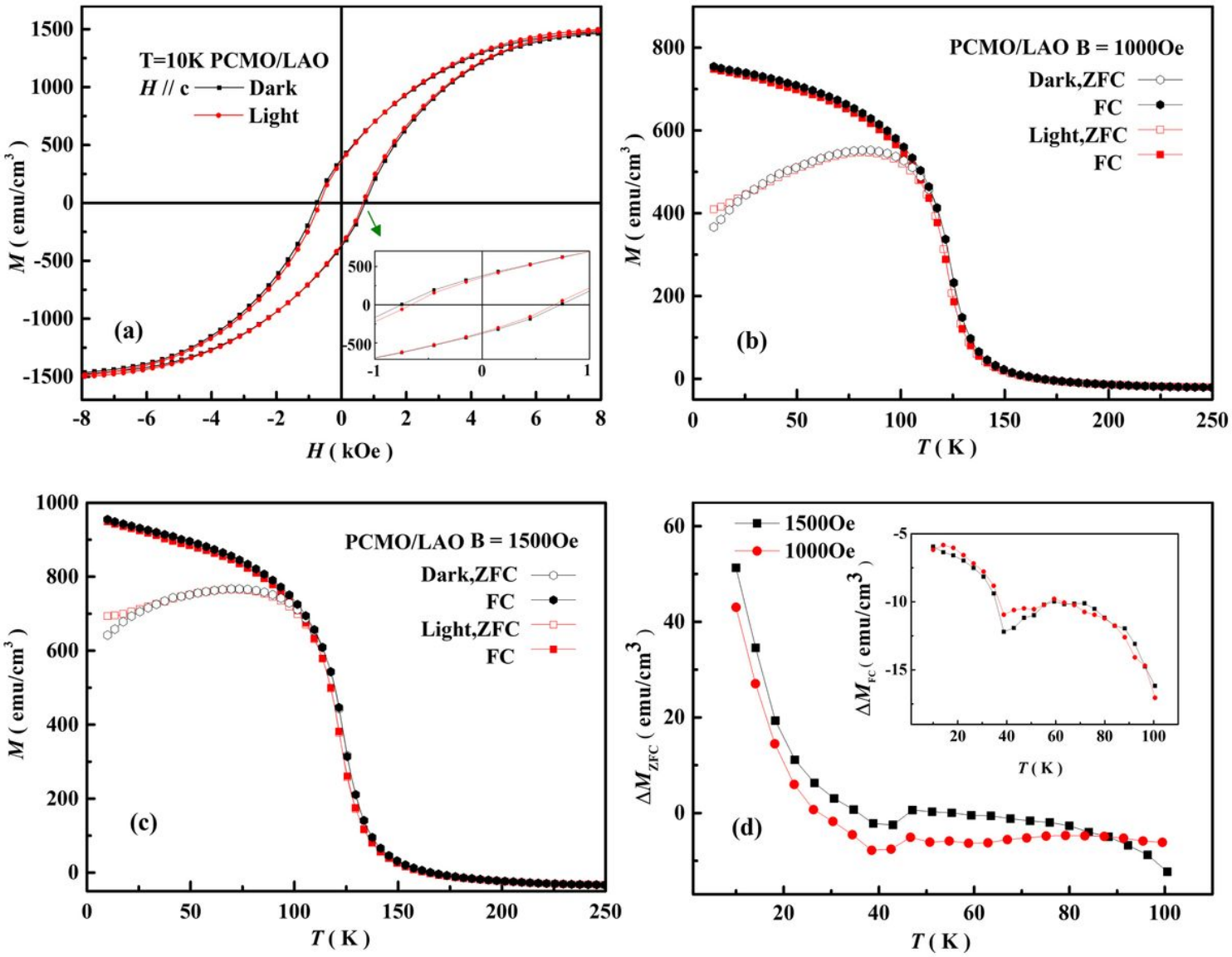

Figure 5

(a) M-H loops in dark and under illumination for PCMO/LAO and the inset is a magnified view of the low-field range. The temperature dependence of the MZFC and MFC magnetizations measured in different magnetic fields of (b) 1000Oe and (c) 1500 Oe before (dark) and during illumination. (d) The magnetization differences of ΔM=ZFClight ^ΔM=ZFCdark in the ZFC case (main panel) and ΔM^FC=MFClight - MFCdark in the FC case (inset).